Associated tW production at CERN LHC: A complete calculation of electroweak supersymmetric effects at one loop

M. Beccaria,[1,2] G. Macorini,[3,4] F. M. Renard,[5] and C. Verzegnassi[3,4]

[1]*Dipartimento di Fisica, Università di Lecce, Via Arnesano, 73100 Lecce, Italy.*
[2]*INFN, Sezione di Lecce*
[3]*Dipartimento di Fisica Teorica, Università di Trieste, Strada Costiera 14, Miramare (Trieste)*
[4]*INFN, Sezione di Trieste*
[5]*Laboratoire de Physique Théorique et Astroparticules, UMR 5207, Université Montpellier II, F-34095 Montpellier Cedex 5*

(Received 20 January 2006; published 8 May 2006)

We compute, in the MSSM framework, the total electroweak contributions at one loop for the process $pp \to tW + X$, initiated by the parton process $bg \to tW$. The supersymmetric effect is analyzed for various choices of the SUSY benchmark points. Choosing realistic unpolarized and polarized experimental quantities, we show the size of the various effects and discuss their dependence on the MSSM parameters.

DOI: 10.1103/PhysRevD.73.093001 PACS numbers: 12.15.−y, 12.15.Lk, 13.75.Cs, 14.80.Ly

I. INTRODUCTION

The relevance of the process of associated tW production from proton-proton collisions has been exhaustively stressed in recent dedicated studies [1]. In the standard model framework, it is well known that accurate measurements of the production rate would provide an excellent determination of the tbW coupling. For physics beyond the standard model (SM), one expects that precision tests of virtual effects might be performed, provided that the effects were *sufficiently* large, i.e. at least of the same size as the overall theoretical and experimental uncertainty. On the theoretical side, an estimate given in [1] predicts for the total production cross section an uncertainty of about 15%. On the experimental side one must recall the fact that the considered process will be seen, for the first time, at LHC, simply because of the required pp energy. Therefore an estimate of the expected experimental uncertainty is in fact still missing. This might be particularly relevant, if the estimated effect turned out to be *reasonable* (e.g. of the same size as the theoretical one), for the special purpose of performing a precision test of supersymmetric models, in particular, of the simplest available one, the minimal supersymmetric standard model (MSSM). In fact, in a previous paper [2], the genuinely weak effects of the model were considered at one loop for all the processes of single top production (td, $t\bar{b}$, tW and also tH^-) at LHC. The treatment was rather preliminary and qualitative, and only considered the very special case of a light SUSY scenario and of a production in a large (~ 1 TeV) final invariant mass range, where a simple logarithmic expansion of so called Sudakov kind could be used. The feature that emerged was that, for the three processes that will certainly be seen at LHC (i.e. td, $t\bar{b}$, tW), the electroweak relative effect in the MSSM is sizable, particularly for large $\tan\beta$ values where it could reach the 30% size. This appeared to us a good motivation for performing a complete accurate estimate, valid for all realistic invariant masses and containing all the parameters of the model. In this paper, we present the results of our effort for the tW production process. It is, to our knowledge, the first complete calculation of the electroweak MSSM effects at one loop for the process, that also includes the QED soft photon radiation. We have checked the validity of our results in three different ways, i.e. (a) we have verified the cancellation of all the (virtual) ultraviolet divergences, (b) we have verified the cancellation of all the (real and virtual) infrared divergences and, last but not least, (c) we have verified the exact reproduction of the asymptotic Sudakov expansions, given in [2], from the computed Feynman diagrams. After these three checks we hope that our results should be correct, and we shall show them in the paper with the following plan: in Sec. II a brief description of the relevant Feynman diagrams is given, and a discussion of the cancellation of the ultraviolet and infrared divergences is provided. Section III shows the reproduction of the (essentially academic) asymptotic Sudakov expansion. In Sec. IV, the realistic observables are defined, and the related MSSM effect is shown for various choices of the SUSY benchmark points. A final discussion that included a review of future calculations is provided in Sec. V.

II. MSSM $bg \to tW$ PRODUCTION AT ONE LOOP

The process that we have considered is the so-called exclusive associated tW production, whose partonic description corresponds to the two body final state reaction

$$bg \to tW^-, \tag{1}$$

that is represented, at Born level, in Fig. 1. In this paper we shall not consider the inclusive process

$$gg \to t\bar{b}W^-. \tag{2}$$

As known [3], the collinear $\bar{b}$ component of this process is already enclosed as a QCD NLO correction to the bottom quark distribution function of the exclusive process Eq. (1)

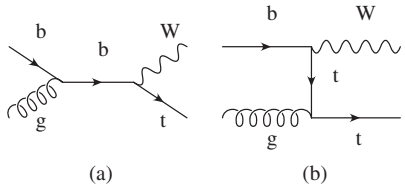

FIG. 1. Born diagrams for the process $bg \to tW^-$.

and our treatment will only consider the one-loop electroweak effects.

At the one-loop level, we have to consider different kinds of Feynman diagrams, several of which will exhibit an ultraviolet divergence. We shall choose the *on-shell* renormalization scheme, and in this framework we shall define the following classes of Feynman diagrams:

A. Born, self-energies and counterterms

The two Born diagrams represented in Fig. 1(a) and 1(b) are an s-channel b quark exchange and a u-channel top quark exchange. With the definitions $s = (p_b + p_g)^2 = (p_W + p_t)^2$, and $u = (p_b - p_W)^2 = (p_g - p_t)^2$ channel, we have

$$A^{\mathrm{Born}}(gb \to Wt) = \frac{eg_s}{s_W\sqrt{2}}\bar{u}(t)\left[\frac{\not\epsilon P_L(\not q + m_b)\not e}{s - m_b^2} + \frac{\not e(\not q' + m_t)\not\epsilon P_L}{u - m_t^2}\right]u(b) \tag{3}$$

where

$$\begin{aligned} q &= p_g + p_b = p_W + p_t \qquad s = q^2 \\ q' &= p_t - p_g = p_b - p_W \qquad u = q'^2, \end{aligned} \tag{4}$$

and e, ϵ are the gluon and W polarization vectors, respectively.

In the on-shell renormalization scheme, these Born terms have to be completed with counterterms associated to the b, t, and W lines. These counterterms are expressed in terms of quark and gauge bosons self-energy functions $\Sigma^f_{L,R,S}(k^2)$, $\Sigma^{VV'}(k^2)$. In these self-energies we take into account SM and SUSY contributions (sfermions, Higgs, neutralinos and charginos) [4]. The b and t quark propagators are also modified by self-energy functions of s and u.

In the s-channel, we can use the invariant forms

$$I^s_{1L,R} = \not\epsilon\not q\not e P_{L,R} \qquad I^s_{2L,R} = \not\epsilon\not e P_{L,R}, \tag{5}$$

and write the amplitude as

$$A = \sum_\eta \{N^s_1 I^s_{1\eta} + N^s_2 I^s_{2\eta}\}, \tag{6}$$

where

$$N^s_1 = \frac{eg_s}{\sqrt{2}s_W(s - m_b^2)}\left\{1 + \delta Z^W_1 - \delta Z^W_2 + \frac{1}{2}\delta\Psi_W + \frac{1}{2}\delta\Psi_t + \frac{3}{2}\delta Z^b_L + \frac{1}{2}\delta Z^t_L - \frac{s}{s - m_b^2}(\Sigma^b_L(s) + \delta Z^b_L) - \frac{m_b^2}{s - m_b^2}(\Sigma^b_R(s) + \delta Z^b_R) - \frac{2m_b^2}{s - m_b^2}\left[\Sigma^b_S(s) - \frac{1}{2}(\delta Z^b_L + \delta Z^b_R) - \frac{\delta m_b}{m_b}\right]\right\} \tag{7}$$

$$N^s_1 = 0 \qquad N^s_2 = 0 \tag{8}$$

$$N^s_2 = \frac{eg_s m_b}{\sqrt{2}s_W(s - m_b^2)}\left\{1 + \delta Z^W_1 - \delta Z^W_2 + \frac{1}{2}\delta\Psi_W + \frac{1}{2}\delta\Psi_t + \frac{1}{2}\delta Z^b_L + \frac{1}{2}\delta Z^t_L + \delta Z^b_R - \frac{s}{s - m_b^2}(\Sigma^b_R(s) + \delta Z^b_R + \Sigma^b_L(s) + \delta Z^b_L) - \frac{s + m_b^2}{s - m_b^2}\left[\Sigma^b_S(s) - \frac{1}{2}(\delta Z^b_L + \delta Z^b_R) - \frac{\delta m_b}{m_b}\right]\right\}. \tag{9}$$

In the u-channel, we define

$$I^u_{1L,R} = \not\epsilon\not q'\not\epsilon P_{L,R} \qquad I^u_{2L,R} = \not\epsilon\not\epsilon P_{L,R}, \tag{10}$$

and write

$$A = \sum_\eta \{N^u_1 I^u_{1\eta} + N^u_2 I^u_{2\eta}\}, \tag{11}$$

with

$$N_1^u = \frac{eg_s}{\sqrt{2}s_W(u-m_t^2)}\Big\{1+\delta Z_1^W-\delta Z_2^W+\frac{1}{2}\delta\Psi_W+\frac{1}{2}\delta\Psi_t+\frac{3}{2}\delta Z_L^t+\frac{1}{2}\delta Z_L^b-\frac{u}{u-m_t^2}(\Sigma_L^t(u)+\delta Z_L^t)$$
$$-\frac{m_t^2}{u-m_t^2}(\Sigma_R^t(u)+\delta Z_R^t)-\frac{2m_t^2}{u-m_t^2}\Big[\Sigma_S^t(u)-\frac{1}{2}(\delta Z_L^t+\delta Z_R^t)-\frac{\delta m_t}{m_t}\Big]\Big\} \tag{12}$$

$$N_1^u = 0 \qquad N_2^u = 0 \tag{13}$$

$$N_2^u = \frac{eg_s m_t}{\sqrt{2}s_W(u-m_t^2)}\Big\{1+\delta Z_1^W-\delta Z_2^W+\frac{1}{2}\delta\Psi_W+\frac{1}{2}\delta\Psi_t+\frac{1}{2}\delta Z_L^b+\frac{1}{2}\delta Z_L^t+\delta Z_R^t$$
$$-\frac{u}{u-m_t^2}(\Sigma_R^t(u)+\delta Z_R^t+\Sigma_L^t(u)+\delta Z_L^t)-\frac{u+m_t^2}{u-m_t^2}\Big[\Sigma_S^t(u)-\frac{1}{2}(\delta Z_L^t+\delta Z_R^t)-\frac{\delta m_t}{m_t}\Big]\Big\}. \tag{14}$$

The various counterterms have the following explicit expressions in terms of self-energies. First, we have the divergent quark wave function renormalizations

$$\delta Z_L^b = \delta Z_L^t \equiv \delta Z_L$$
$$= -\Sigma_L^b(m_b^2) - m_b^2[\Sigma_L'^b(m_b^2)+\Sigma_R'^b(m_b^2)+2\Sigma_S'^b(m_b^2)] \tag{15}$$

$$\delta Z_R^b = -\Sigma_R^b(m_b^2) - m_b^2[\Sigma_L'^b(m_b^2)+\Sigma_R'^b(m_b^2)+2\Sigma_S'^b(m_b^2)] \tag{16}$$

$$\delta Z_R^t = \delta Z_L + \Sigma_L^t(m_t^2) - \Sigma_R^t(m_t^2). \tag{17}$$

Then, we have the finite wave function renormalization required in the on-shell scheme and unavoidable since we have both up and down type quarks in the process

$$\delta\Psi_t = -\{\Sigma_L^t(m_t^2)+\delta Z_L+m_t^2[\Sigma_L'^t(m_t^2)+\Sigma_R'^t(m_t^2)$$
$$+2\Sigma_S'^t(m_t^2)]\}. \tag{18}$$

The similar terms for the W gauge boson are

$$\delta Z_1^W - \delta Z_2^W = \frac{\Sigma^{\gamma Z}(0)}{s_W c_W M_Z^2}, \tag{19}$$

$$\delta Z_2^W = -\Sigma'^{\gamma\gamma}(0)+2\frac{c_W}{s_W M_Z^2}\Sigma^{\gamma Z}(0)+\frac{c_W^2}{s_W^2}\Big[\frac{\delta M_Z^2}{M_Z^2}-\frac{\delta M_W^2}{M_W^2}\Big], \tag{20}$$

and

$$\delta\Psi_W = -\Sigma'^{WW}(M_W^2) = -\{\Sigma'^{WW}(M_W^2)+\delta Z_2^W\}. \tag{21}$$

Finally, we list the mass counterterms

$$\delta M_W^2 = Re\Sigma^{WW}(M_W^2) \qquad \delta M_Z^2 = Re\Sigma^{ZZ}(M_Z^2) \tag{22}$$

$$\delta m_b = \frac{m_b}{2}Re[\Sigma_L^b(m_b^2)+\Sigma_R^b(m_b^2)+2\Sigma_S^b(m_b^2)] \tag{23}$$

$$\delta m_t = \frac{m_t}{2}Re[\Sigma_L^t(m_t^2)+\Sigma_R^t(m_t^2)+2\Sigma_S^t(m_t^2)]. \tag{24}$$

B. Vertex corrections and box diagrams

The next two classes of diagrams are trianglelike vertices and box diagrams. A list of the generic diagrams (i.e. diagrams with virtual particles left unspecified apart from their spin) is shown in Fig. 2 as produced by FeynArts [5]. Schematically we can further subdivide them as follows (q stands for b or t quarks, V for γ, Z, W, H for neutral or charged Higgses or Goldstone particles, χ for chargino or neutralino):

(1) *Initial* s-channel triangles connected to the intermediate b quark: (Vqq), (Hqq), $(\chi\tilde{q}\,\tilde{q})$;
(2) *Final* s-channel triangles connected to the intermediate b quark: (btV), (HHq), $(\tilde{b}\,\tilde{t}\,\chi)$ (VVq), (HVq), (VHq), (btH), $(\chi\chi\tilde{q})$;
(3) *Up* u-channel triangles connected to the intermediate t quark: (qqV), (qqH), $(\tilde{q}\,\tilde{q}\,\chi)$,
(4) *Down* u-channel triangles connected to the intermediate t quark: (tbV), (tbH), $(\chi\chi\tilde{q})$, (VVq), (VHq), (HVq), (HHq), $(\tilde{t}\,\tilde{b}\,\chi)$;
(5) *Direct* boxes: $(\tilde{b}\,\tilde{b}\,\tilde{t}\,\chi^0)$, $(bbtV)$, $(bbtH)$;
(6) *Crossed* boxes: $(qqVV)$, $(qqVH)$, $(qqHV)$, $(qqHH)$, $(\tilde{q}\,\tilde{q}\,\chi\chi)$;
(7) *Twisted* boxes: $(ttVb)$, $(ttHb)$, $(\tilde{t}\,\tilde{t}\,\chi^0\tilde{b})$.

The notation corresponds to the clockwise ordering of the internal particles inside the diagrams.

An essential step consists then in checking the cancellation of UV divergences. They appear in the self-energy functions $\Sigma(k^2)$, in the various counterterms, and in the various triangles. Box contributions are convergent. We have checked the cancellation when summing all of these terms. This cancellation occurs in several independent sectors (gauge, Higgs, SM, SUSY).

Having completed the first important check (cancellation of UV divergences) we now move to the forthcoming

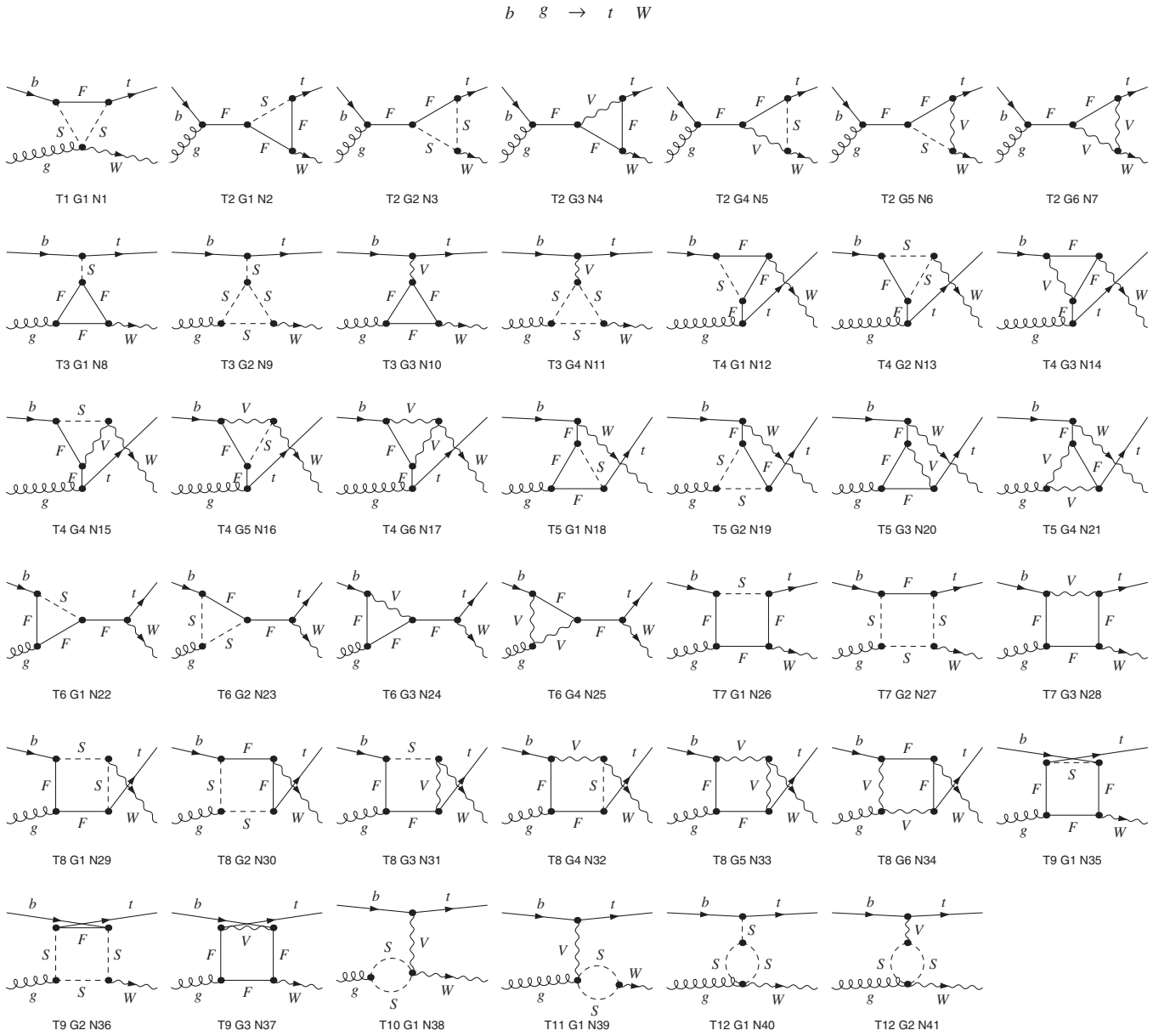

FIG. 2. Generic diagrams for the process $bg \to tW^-$. We list only the vertex corrections and the box diagrams. The labels S, F, and V denote generic particles with spin 0, $1/2$, and 1.

issue of cancellation of IR divergences that will be treated in the forthcoming discussion.

C. Cancellation of IR divergences

QED radiation effects are usually split into a soft part containing the potential IR singular terms, and a hard part including the emission of photons with energy not small compared to the process energy scale. In this brief section, we discuss the soft emission and the detailed cancellation of IR divergences that occurs when it is combined with virtual photon exchanges.

Let us denote by $\mathcal{A}^{\text{Born}}$ and $\mathcal{A}^{1\,\text{loop}}$ any invariant helicity scattering amplitude evaluated at Born or one loop level. Let us also denote by λ the photon mass acting as an IR regulator. The IR cancellation between (soft) real radiation and virtual photon exchange holds in every helicity channel separately and we have checked it numerically.

It reads

$$(\mathcal{A}^{\text{Born}})^2\left(1+\frac{\alpha}{2\pi}\delta_s\right)+2\mathcal{A}^{\text{Born}}\mathcal{A}^{1\,\text{loop}}=\text{finite as } \lambda\to 0, \tag{25}$$

where, in the above expressions, δ_S is the correction factor taking into account the emission of soft real photons with

energy from λ up to $E_\gamma^{\max} \ll \sqrt{s}$. The explicit expression for δ_S can be found, for instance, in [6].

In practice the above relation follows from the eikonal factorization

$$\mathcal{A}^{\text{1 loop}} = -\mathcal{A}^{\text{Born}} \frac{\alpha}{4\pi} \delta_s + \text{regular terms as } \lambda \to 0. \tag{26}$$

It is possible to split further the above factorization property. Indeed, the singular part of the radiation factor has the form

$$\delta_S = \log\frac{\lambda}{E_\gamma^{\max}} \sum_{i,j} \delta_S^{i,j} + \text{regular terms as } \lambda \to 0, \tag{27}$$

where i and j runs over the initial/final charged particles, i.e. (bt), (bW), and (tW). There are two types of contributions: the diagonal ones with $i = j$ and the off-diagonal ones with $i \neq j$ [6].

Now, the matching between the singular $\log\lambda$ in the left-hand side and right-hand side of Eq. (26) can be checked in several independent steps as follows

(1) the diagonal radiation terms $i = j$ match the IR divergence in the counterterms associated to the i-th external line [7].
(2) the off-diagonal radiation terms $i \neq j$ match the IR divergence in the diagrams which are obtained connecting in all ways the i-th and j-th external lines with a virtual photon. This operation produces both triangle and box diagrams.

As a final comment, we remark that gauge invariance is crucial to cancel all nonfactoring contributions associated to the final W line as discussed in [8].

The next step in the treatment of QED effect is the calculation of hard photon emission. We have left this subject to a dedicated study which shall be discussed separately [9].

III. SUDAKOV EXPANSION OF THE SCATTERING AMPLITUDES

Let us now consider the high energy behavior of the $bg \to tW$ helicity amplitudes $F_{\lambda\mu\lambda'\mu'}$, where λ, μ, λ', μ' refer to the helicities λ_b, λ_g, λ_t, λ_W respectively. Several simplifications appear in the Born and in the one-loop contributions. When $s \gg m_i^2$ (m_i being the internal or external involved masses), ignoring m_i^2/s contributions, the nonsuppressed Born amplitudes reduce to F_{----}, F_{-+-+} for transverse W and F_{-++0} for longitudinal W.

The leading high energy Born helicity amplitudes are

$$F^{\text{Born}}_{----} \to \frac{eg_s}{s_W\sqrt{2}}\left(\frac{\lambda^l}{2}\right)\frac{2}{\cos\frac{\theta}{2}} \tag{28}$$

$$F^{\text{Born}}_{-+-+} \to \frac{eg_s}{s_W\sqrt{2}}\left(\frac{\lambda^l}{2}\right)2\cos\frac{\theta}{2} \tag{29}$$

$$F^{\text{Born}}_{-++0} \to \frac{eg_s}{s_W}\left(\frac{\lambda^l}{2}\right)\frac{m_t}{M_W}\cos\frac{\theta}{2}\left(\frac{1-\cos\theta}{1+\cos\theta}\right). \tag{30}$$

Note that F_{-++0} is controlled by the top Yukawa coupling factor $\sim m_t/M_W$. In fact the amplitude F_{+--0} also occurs but at a much weaker level as it is controlled by the bottom Yukawa coupling factor $\sim m_b/M_W$.

At one loop, these amplitudes receive logarithmic enhancements as discussed in several papers, called Sudakov terms. These terms are separated into universal and into angular dependent components. From the rules established in [10], one expects the following expressions (there are misprints in the paper [2]; The correct equations are the following Eqs. (31)–(46)).

For transverse W amplitudes:

$$F^{\text{Univ}}_{-,\mu,-,\mu} = F^{\text{Born}}_{-,\mu,-,\mu}\left[\frac{1}{2}(c^{ew}(b\bar{b})_L + c^{ew}(t\bar{t})_L) + c^{ew}(W_T)\right] \tag{31}$$

$$c^{ew}(q\bar{q})_L = c^{ew}(\tilde{q}\,\tilde{\bar{q}})_L = c(q\bar{q}, \text{gauge})_L + c(q\bar{q}, \text{yuk})_L \tag{32}$$

$$c(d\bar{d}, \text{gauge})_L = c(u\bar{u}, \text{gauge})_L = \frac{\alpha(1+26c_W^2)}{144\pi s_W^2 c_W^2}\left(n\log\frac{s}{m_W^2} - \log^2\frac{s}{m_W^2}\right) \tag{33}$$

$$c(d\bar{d}, \text{gauge})_R = \frac{\alpha}{36\pi c_W^2}\left(n\log\frac{s}{m_W^2} - \log^2\frac{s}{m_W^2}\right) \tag{34}$$

$$c(u\bar{u}, \text{gauge})_R = \frac{\alpha}{9\pi c_W^2}\left(n\log\frac{s}{m_W^2} - \log^2\frac{s}{m_W^2}\right), \tag{35}$$

where $n = 3, 2$ in SM and MSSM, respectively.

$$c(b\bar{b}, \text{yuk})_L = c(t\bar{t}, \text{yuk})_L = -\frac{\alpha}{16\pi s_W^2}\left[\log\frac{s}{m_W^2}\right]\left[\frac{m_t^2}{m_W^2}y_t + \frac{m_b^2}{m_W^2}y_b\right] \tag{36}$$

$$c(b\bar{b}, \text{yuk})_R = -\frac{\alpha}{8\pi s_W^2}\left[\log\frac{s}{m_W^2}\right]\left[\frac{m_b^2}{m_W^2}y_b\right] \tag{37}$$

$$c(t\bar{t}, \text{yuk})_R = -\frac{\alpha}{8\pi s_W^2}\left[\log\frac{s}{m_W^2}\right]\left[\frac{m_t^2}{m_W^2}y_t\right], \tag{38}$$

where $y_t = 1,\ 2(1+\cot^2\beta)$ and $y_b = 1,\ 2(1+\tan^2\beta)$ in SM and MSSM, respectively.

$$c^{ew}(W_T) = \frac{\alpha}{4\pi s_W^2}\left[-\log^2\frac{s}{M_W^2}\right], \tag{39}$$

and for the longitudinal W_0^- amplitude:

$$F^{\text{Univ}}_{-,+,+,0} = F^{\text{Born}}_{-,+,+,0}\left[\frac{1}{2}(c^{ew}(b\bar{b})_L + c^{ew}(t\bar{t})_R) + c^{ew}(W_0)\right], \tag{40}$$

with, in SM:

$$c^{ew}(W_0) = \frac{\alpha}{4\pi}\left\{\left[-\frac{1+2c_W^2}{8s_W^2c_W^2}\log^2\frac{s}{M_W^2}\right] + \left[\log\frac{s}{M_W^2}\right] \times\left[-\frac{15-42c_W^2}{72s_W^2c_W^2} + \frac{3(m_t^2-m_b^2)}{8s_W^2M_W^2}\right]\right\}, \tag{41}$$

such that

$$F^{\text{Univ}}_{-,+,+,0} = F^{\text{Born}}_{-,+,+,0}\left[\frac{\alpha}{4\pi}\right]\left\{\left[-\log^2\frac{s}{M_W^2}\right]\left[\frac{13+14c_W^2}{36s_W^2c_W^2}\right] + \left[\frac{1+2c_W^2}{2s_W^2c_W^2} - \frac{m_b^2}{2s_W^2c_W^2}\right]\left[\log\frac{s}{M_W^2}\right]\right\}, \tag{42}$$

whereas in MSSM:

$$c^{ew}(W_0) = \frac{\alpha}{4\pi}\left\{\left[-\frac{1+2c_W^2}{8s_W^2c_W^2}\log^2\frac{s}{M_W^2}\right] + \left[\log\frac{s}{M_W^2}\right] \times\left[-\frac{17+10c_W^2}{36s_W^2c_W^2} + \frac{m_b^2}{4s_W^2M_W^2}(1+\tan^2\beta) + \frac{3m_t^2}{4s_W^2M_W^2}(1+\cot^2\beta)\right]\right\}, \tag{43}$$

such that

$$F^{\text{Univ}}_{-,+,+,0} = F^{\text{Born}}_{-,+,+,0}\left[\frac{\alpha}{4\pi}\right]\left\{\left[-\log^2\frac{s}{M_W^2}\right]\left[\frac{13+14c_W^2}{36s_W^2c_W^2}\right]\right\}, \tag{44}$$

(in which all single logs cancel).

For the electroweak angular terms we find:

$$F^{\text{ang}}_{-,\mu,-,\mu} = F^{\text{Born}}_{-,\mu,-,\mu}\left[-\frac{\alpha}{2\pi}\right]\left[\log\frac{s}{M_W^2}\right]\left\{\left[\log\frac{-t}{s}\right] \times\left[\frac{1-10c_W^2}{36s_W^2c_W^2}\right] + \frac{1}{s_W^2}\log\frac{-u}{s}\right\} \tag{45}$$

$$F^{\text{ang}}_{-,+,+,0} = F^{\text{Born}}_{-,+,+,0}\left[-\frac{\alpha}{24\pi c_W^2}\right]\left[\log\frac{s}{M_W^2}\right]\left\{\left[\frac{4}{3}\log\frac{-t}{s}\right] - \frac{1-10c_W^2}{s_W^2}\log\frac{-u}{s}\right\}. \tag{46}$$

Note that the longitudinal W amplitudes satisfy the equivalence theorem which states that, neglecting m_i^2/s contributions, they should coincide with the amplitudes for the process $bg \to tG^-$, G^- being the charged Goldstone boson.

We have checked that our full one-loop result reproduces the logarithmic contributions predicted by the above rules. This check is straightforward and can be performed by expanding the various B, C, D Passarino-Veltman functions appearing in the self-energy, triangle, and box-type amplitudes.

These resulting asymptotic expressions deserve several comments. In the case of transverse W production, one checks that at Born and one-loop level and at next-to-leading logarithmic accuracy in addition to trivial fermion chirality constraint $\lambda_t = \lambda_b = -1/2$ gauge boson helicity conservation [11] is preserved, both in SM and MSSM cases, i.e. only $\mu = \mu'$ amplitudes survive. One then sees that the MSSM differs from the SM in the single logarithm contributions, $n = 2$ instead of $n = 3$ for gauge terms and $2(1 + \cot^2\beta)$ or $2(1 + \tan^2\beta)$ Yukawa enhancements, especially large for large $\tan\beta$.

In the case of longitudinal W production, the Born amplitude is controlled by the Yukawa m_t/M_W factor associated to fermion chirality violation $\lambda_t = -\lambda_b = 1/2$ and satisfies also the rule $\lambda_g + \lambda_b = \lambda_t$ which is an extension of the GBHC rule [11]. An additional remarkable feature appears for the single log contribution, namely, it totally cancels in the MSSM case.

Having successfully performed the ultraviolet, infrared and Sudakov *tests*, we hope that our complete expressions will be correct. In this respect, we should add the following comment: We do not expect that, at lower energies and for higher SUSY masses, the simple features that we met in the *light SUSY* Sudakov description given in [2] retain their full validity. Still, we would expect that at least some of the main features could survive. For instance, for what concerns the slope of the invariant mass distribution, we could hope that a simple modification at lower energies, or at lower energy/SUSY masses ratios, might be the addition of a (possibly *large*) constant term at least in a *moderate* energy region not too far from the asymptotic one, so that a smooth connection between the two regions is achieved. In the following section we shall return on this point, but first we shall define and examine those quantities that will be the realistic experimental observables.

IV. PHYSICAL PREDICTIONS

We are now able to provide numerical predictions for the complete electroweak effect of the MSSM at one loop on the realistic observables of the considered tW production process. The numerical evaluation of the scattering amplitude has been performed with the help of the LoopTools library [12]. We shall divide our presentation in two parts that correspond, respectively, to the consideration of unpolarized and of polarized quantities. Following a pragmatic attitude i.e. assuming that only unpolarized observables will be measured in a first stage of the experiments, we shall start our analysis with the former ones.

The first quantity that we shall consider is the invariant mass distribution, conventionally defined as

$$\frac{d\sigma(PP \to tW^- + X)}{ds} = \frac{1}{S}\int_{\cos\theta_{\min}}^{\cos\theta_{\max}} d\cos\theta\Big[L_{bg}(\tau,\cos\theta) \times \frac{d\sigma_{bg\to tW^-}}{d\cos\theta}(s)\Big], \quad (47)$$

where $\tau = \frac{s}{S}$, and L_{bg} is the parton process luminosity.

$$L_{bg}(\tau,\cos\theta) = \int_{\bar{y}_{\min}}^{\bar{y}_{\max}} d\bar{y}\Big[b(x)g\Big(\frac{\tau}{x}\Big) + g(x)b\Big(\frac{\tau}{x}\Big)\Big], \quad (48)$$

where S is the total pp c.m. energy, and $i(x)$ the distributions of the parton i inside the proton with a momentum fraction, $x = \sqrt{\frac{\tau}{S}}e^{\bar{y}}$, related to the rapidity $\bar{y}$ of the tY system [13]. The parton distribution functions are the latest LO MRST (Martin, Roberts, Stirling, Thorne) set available on [14]. The limits of integrations for $\bar{y}$ depends on the cuts. We have chosen a maximal rapidity $Y = 2$ and a minimum p_T which we shall specify later.

Note that we are at this stage considering as kinematical observable the initial partons c.m. energy $\sqrt{s}$, and not the realistic final state invariant mass M_{tW}. The transition from the first quantity to the second one can be performed using the available suitable event generators, like for instance PYTHIA [15], as we did in a previous paper on top-antitop production [16]. We expect from that experience a small (few percent) modification in the transition from $\sqrt{s}$ to M_{tW}. This correction can be considered as a *QCD effect*, and as such it will be consistently treated in a forthcoming paper [17] where this type of nonelectroweak effects will be included. For what concerns the complete one-loop electroweak amplitude, we can compute it for any choice of the MSSM parameters, but before doing this we want to show some features of the simple Born approximation of the partonic amplitude that we consider particularly relevant for an understanding of our following results. More precisely, the point that we want to stress is that the partonic invariant scattering amplitude for the process, that represents the starting block of our calculations, turns out to be the sum of 12 different helicity amplitudes, that have been defined already in Sec. III. For large values of $\sqrt{s}$, i.e. for $\sqrt{s}$ sufficiently larger than the masses of all the particles and sparticles involved in the one-loop description of the process, we expect that only three helicity amplitudes remain dominant, more precisely those that have been defined in Sec. III as F_{----}, F_{-+-+}, F_{-++0} (the third and fourth index specifies the top and W helicity). The remaining helicity amplitudes vanish asymptotically i.e. for $s \to \infty$ like $1/s$ with possible logarithmic corrections at one loop, and in our preliminary paper [2] they were systematically neglected in the region of that was considered, corresponding to a) energies in the 1 TeV range and b) *light* SUSY masses scenario. For the realistic analysis that we can now carry on, both assumptions will be abandoned. In particular:

(a) The possibility of identifying the final (t, W) signal must face the serious competition of a background, mostly due to events coming from the copious top-antitop and WWj production. This problem has been already exhaustively discussed in a previous paper [3], where it has been shown that the introduction of suitable b-tagging cuts will allow to extract the signal at reasonable (20 fb^{-1}) luminosities. *A priori,* one would expect that the background contamination should be under control for c.m. energies below a qualitative *background threshold* of approximately, say, 400–500 GeV, and increase in the higher energies region. Keeping this limitation in mind, we have nonetheless analyzed in this paper the full energy region from threshold to 1 TeV, although at this final energy value the identification of the signal might be difficult. The reason of this (optimistic) choice is that we do not have yet at disposal a rigorous experimental analysis of the realistically expected size of the signal at variable energies, as we had in the preliminary top-antitop paper [16]. This analysis is being already performed, and will be included in the already mentioned forthcoming work.

(b) The SUSY scenario that we shall investigate is the conventional mSUGRA one. In particular, we shall consider a number of benchmark points that are nowadays available, trying to choose those that show a definite difference in the values of the various SUSY masses, and of $\tan\beta$. We insist on the fact that we could perform its calculation for any choice of the parameters, but for obvious reasons we have limited the presentation of figures in this paper.

After these preliminary remarks, we now show in Fig. 3 the comparison (treated in Born approximation) of quantities that we consider particularly worth of being considered, i.e. the parton c.m. angular dependences of the differential cross section in various helicity channels. We have chosen four c.m. energy values, $\sqrt{s} = 300, 500, 1000,$ and (academically) 2000 GeV and retained for sake of comparison the full angular range $-1 \le \cos\theta \le 1$ (possible angular cuts will be considered separately). We have only retained those terms that are numerically meaningful, leaving aside the *invisible* ones. In the Figure, for simplicity, we show only the 5 amplitudes which are leading at high energy. These are the three asymptotic ones generated by the helicity amplitudes previously defined and two extra ones, corresponding to F_{---0} and F_{-++-}. The important points to be noticed are the following ones:

(1) The relative relevance of the different helicity differential cross sections changes drastically with the scattering angle for the two lower energy points. As one sees, the scattering in the nearly backward region is totally dominated for $\sqrt{s} = 300$–500 GeV by the two *nonasymptotic* quantities; the weight of

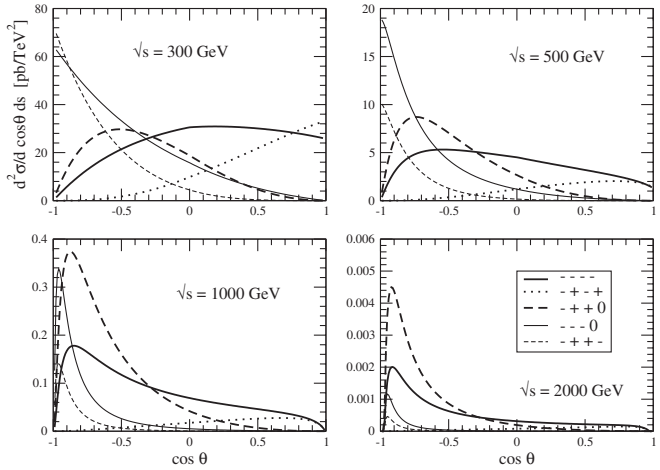

FIG. 3. We show the energy and angular dependence of the 5 helicity amplitudes which are leading at high energy. Of course, these include the three amplitudes which are not mass suppressed. In addition, we show the next relevant amplitudes which are the mass suppressed ones F_{---0} and F_{-++-}. An inspection of the Figure shows that below 1 TeV the mass suppression is not effective, especially in the backward region.

the asymptotic differential cross sections becomes dominant when θ moves to the forward direction, where the overall numerical size is, though, smaller than that of the backward region.

(2) Although less evidently, these features survive also at the next energy point $\sqrt{s} = 1$ TeV. More precisely, the size of the F_{---0} distribution remains essential in the backward region.

(3) One might start doubting about the validity of our asymptotic assumptions. To show that this is not the case, we have plotted the distributions in the last subfigure, for the (academic) point $\sqrt{s} = 2$ TeV. As one sees, the features at this energy are those that would expect at (sufficiently!) high energies: the largely dominant contribution is that of two of the asymptotic quantities, more precisely F_{-++0} and F_{----}.

In conclusion, we see that the contribution of the *non-asymptotic* helicity amplitudes, for which no Sudakov expansion has to be expected, is essential for realistic (i.e., qualitatively <1 TeV) energies. A *proper* asymptotic behavior seems to eventually set in, but only at higher energies (say, ~ 2 TeV), where the possibility of detecting the signal appears, least to say, debatable. Although these features were derived by an analysis performed in Born approximation, we expect that the complete results that will follow will be consistent with these preliminary impressions.

V. RESULTS

The successful results of our previous tests have encouraged us to prepare with a reasonable amount of confidence a numerical C + + code that contains the complete *tested* one-loop expression of all the components of the considered process. This program has been called MINSTREL and is nowadays working and available. Thanks to this code we are now able to provide numerical predictions for the complete electroweak effect of the MSSM at one loop on the realistic observables of the associated tW^- production.

With this aim, we have returned to Eq. (47) and have considered a set of SUSY benchmark points that appeared to us suited for our analysis. More precisely, we have retained representative points whose SUSY masses values are not *light* (but not even dramatically large) and also points whose masses are, conversely, *light* (in our language, lighter than, say, 400–500 GeV). Also, we have used points whose only essential difference is the value of $\tan\beta$, that is allowed to become definitely large (50) in one of the two cases and still appreciable (10) in the second one. In this way, we should be able to compare the complete results with those that we found in the *light SUSY* Sudakov approximation. For practical reasons, we will only show the results of our analysis for a choice of four representative points. Two of them are the ATLAS DC2 SU1 and SU6 points [18]; the remaining two are two points whose spectrum has been evaluated by the code SUSPECT [19] and that we have called LS1, LS2 where LS stands for Light SUSY. To make the reasons of our choice evident, we have given in Table I the values of the various SUSY masses, and of $\tan\beta$, that correspond to the four choices. One sees that the first two points correspond to a *not light* choice, with two different values of $\tan\beta$; for the last two points, a *light* SUSY scenario is assumed, with, again, two different $\tan\beta$ values. Two final technical points have to be now added:

(a) Our calculations have been performed with a value of $p_{T,\min} = 15$ GeV.

(b) In the calculations, we have included a QED soft photon contribution, computed assuming an upper value of the soft photon energy $\Delta E = 0.1$ GeV. As we anticipated, the full treatment of the essentially standard model hard photon emission will be contained in a dedicated paper [9].

A. Unpolarized observables

1. Effects in the distribution $d\sigma/ds$

We can now show the first results of our calculations. In Fig. 4 we have drawn the relative effect at one loop of the MSSM, and also of the SM alone, for the four choices of benchmark points. The calculation stops at $\sqrt{s} = 1$ TeV as we announced. From a glance at the different figures, a number of (preliminary) conclusions can already be drawn. In particular:

(a) The *genuine* SUSY effect, i.e. the difference between the MSSM and the SM, remains systematically small (a relative few percent) for all choices of

TABLE I. Table of spectra for the various benchmark points. All entries with the dimension of a mass are expressed in GeV. The spectra have been computed with the code SUSPECT [19].

	SU1	SU6	LS1	LS2
m_0	70	320	300	300
$m_{1/2}$	350	375	150	150
A_0	0	0	−500	−500
$\tan\beta$	10	50	10	50
$\mu/\lvert\mu\rvert$	1	1	1	1
α	−0.110	−0.0212	−0.109	−0.015
M_1	144.2	155.8	60.1	60.6
M_2	270.1	291.3	114.8	115.9
μ	474.4	496.6	329.7	309.3
$H^{\pm}$	534.3	401.7	450.4	228.9
H^0	528.3	392.5	442.5	211.1
h^0	114.6	115.7	111.4	110.8
A^0	527.9	392.5	443.4	212.0
$\chi_1^{\pm}$	262.8	289.3	108.0	111.1
$\chi_2^{\pm}$	495.3	514.8	350.1	329.4
χ_1^0	140.1	153.0	57.38	58.92
χ_2^0	263.1	289.4	108.5	111.3
χ_3^0	479.2	501.0	335.3	315.8
χ_4^0	495.4	514.0	348.7	326.5

	SU1	SU6	LS1	LS2
$\tilde{l}_L$	253.3	412.3	321.0	321.2
$\tilde{l}_R$	157.6	353.4	308.7	308.7
$\tilde{\nu}_e$	241.0	404.8	311.3	311.3
$\tilde{\tau}_L$	149.6	195.8	297.1	078.1
$\tilde{\tau}_R$	256.1	399.2	323.8	282.5
$\tilde{\nu}_\tau$	240.3	362.5	308.4	243.6
$\tilde{u}_L$	762.9	870.5	459.8	460.2
$\tilde{u}_R$	732.9	840.7	451.9	452.3
$\tilde{d}_L$	766.9	874.0	466.4	467.0
$\tilde{d}_R$	730.2	837.8	452.8	453.2
$\tilde{t}_L$	562.5	631.5	213.3	223.6
$\tilde{t}_R$	755.8	796.9	462.9	431.3
$\tilde{b}_L$	701.0	713.7	380.6	304.0
$\tilde{b}_R$	730.2	787.6	449.1	401.7
θ_τ	1.366	1.133	1.091	1.117
θ_b	0.3619	0.7837	0.184	0.653
θ_t	1.070	1.050	1.016	0.9313

the benchmark points in the considered (realistic) energy region. In this sense, a measurement of the invariant mass distribution of the process does not appear to be a promising way of detecting genuine SUSY effects in the MSSM with mSUGRA symmetry breaking (this conclusion could be not valid for different supersymmetric models or symmetry breaking scenarios).

(b) The overall SM plus SUSY one-loop effect, which in the considered case of the MSSM is practically entirely due to the standard model component, is not, though, negligible. As one sees, it varies from positive to negative values in the lowest part of the region, remaining systematically negative for larger energies and reaching a common value of approximately 10% around 1 TeV. This large energy negative shift from the Born level calculation appears a characteristic property of the considered MSSM model, independent of the values of the parameters that were assumed in our analysis. In practice, the fact that the effect is largely dominated by the standard model component of the model is a consequence of the strong decoupling of the genuine SUSY effects that arises in a complete calculation as soon as the sparticle masses assume *not specially light* values, contrary to the assumption made in the preliminary analysis of [2]. It might be that for different supersymmetric scenarios this unlucky cancellation disappears, or becomes less drastic. This possibility, which still remains open at this stage, would deserve in our opinion a further general investigation.

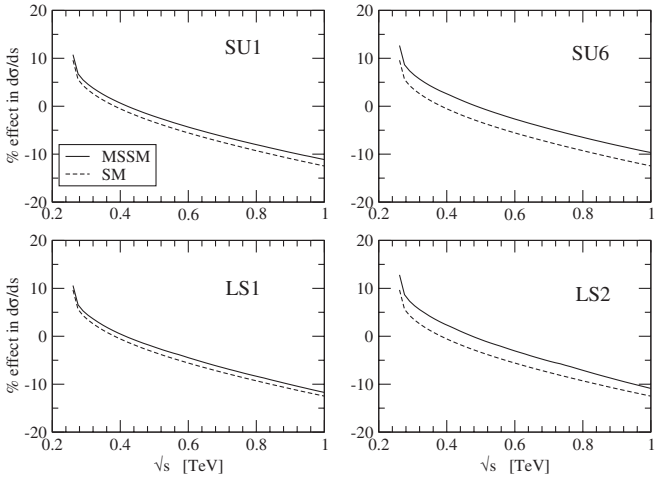

FIG. 4. MSSM and SM one-loop effect in the distribution $d\sigma/ds$ in the four considered scenarios SU1, SU6, LS1, LS2.

(c) In our work, we did not consider QCD corrections as well as their supersymmetric partner corrections involving gluino exchanges. Concerning standard model QCD effects, to our knowledge, they have been recently computed at NLO both for the Tevatron and for the LHC production [20]. At LHC, the effect on the cross section is relatively mild, of the 10% size, i.e. comparable with that of the electroweak corrections. About the genuine SUSY QCD effects, in [2] we computed them in the Sudakov approximation where they contribute additional single logarithms. At full one loop, i.e. including terms not growing with energy, they have not been computed. In principle they are not negligible as indicated by the analysis of the similar

process $bg \to tH^-$ described in [21] and should be included in the complete analysis of standard model and SUSY strong effects which however is beyond the purposes of this paper.

2. Ratios of partially integrated cross sections: A proposal

Since there is a wide energy region where the one-loop effects are appreciable, i.e. $\sqrt{s} \gtrsim 500$ GeV, we can split it in two parts, compute the associated integrated cross section, and evaluate the ratio R of the two partial cross sections. This investigation is motivated by the following remarks concerning general properties of R:

(a) It should be free of several systematic experimental errors;
(b) It should be free of several QCD effects (same pdfs, same virtual corrections);
(c) It should be essentially unaffected by photon radiation effects.

To give an explicit numerical example, we have considered the scenario SU6, and have split the high energy region in two parts:

$$E_{\text{threshold}} \equiv m_t + m_W < \sqrt{s} < 400 \text{ GeV}, \qquad \sqrt{s} > 400 \text{ GeV}. \tag{49}$$

We call σ_- and σ_+ the integrated cross section $\int (d\sigma/ds)\, ds$ in the two regions, and define $R = \sigma_+/\sigma_-$.

We denote by $\varepsilon_\pm$ the relative MSSM effect on the two cross sections. We also denote by $N_\pm$ the expected number of events associated to the two regions. Of course, $N_\pm = \mathcal{L}\sigma_\pm$, where $\mathcal{L}$ is the luminosity. If we call $\Delta_{\text{MSSM}}R$ and $\Delta_{\text{stat}}R$ the MSSM and statistical shifts on R we have

$$\Delta_{\text{MSSM}}R = R(\varepsilon_+ - \varepsilon_-), \qquad \Delta_{\text{stat}}R = R\left(\frac{1}{\sqrt{N_+}} + \frac{1}{\sqrt{N_-}}\right). \tag{50}$$

In our test case, the Born value is $R \simeq 0.58$ and the difference $\varepsilon_+ - \varepsilon_-$ gives a shift of about 3.5%. The purely statistical error computed with a luminosity $\mathcal{L} = 10$ fb^{-1} gives $\Delta_{\text{stat}}R \simeq 0.002$, i.e. a shift about 10 times smaller than the MSSM effect.

We conclude that radiative effects in ratios like R are beyond the statistical noise. Of course, systematic errors are expected to dominate over statistical ones. Thus, a detailed dedicated experimental study of the process reconstruction will be crucial to assess R as a *realistic* observable and a potential precision test of the electroweak sector of the considered MSSM.

3. Sudakov-like parametrizations

To conclude the unpolarized session, we have tried to give an effective parametrization of the full one-loop effect in the spirit of the logarithmic Sudakov expansion. As we remarked, a straightforward comparison with the results described in Sec. III is hampered by a variety of problems, that we now emphasize:

(a) Box diagrams are functions of the Mandelstam invariants t, u beside s. At small or large angles, these can be small (compared to the internal squared masses and s) and spoil the validity of the Sudakov approximation.
(b) At high but moderate energies (below 1 TeV) there are several subleading helicity channels which are relevant and non-negligible. These channels certainly admit a Sudakov expansion. However this is not as simple as that of the leading channels. The coefficients of the expansion for these amplitudes have not been investigated before and could or could not turn out to be simple combination of quantum numbers and couplings as in the leading case.
(c) In the MSSM, we have sparticles with masses around 300–400 GeV, even in the lightest considered scenario LS2. The extent to which they can be regarded as *small* can only be determined by an explicit numerical comparison of the two calculations. Indeed, by a careful inspection of the various involved diagrams one sees that box diagrams can display a rather delayed asymptotic behavior. In practice, if the typical virtual masses are of order m, there are box diagrams with asymptotic behavior $\sim \log(\sqrt{s}/m')$ where m' can be 4–5 times larger than m, depending, in particular, on the scattering angle. This large effective scale contributes a large energy independent constant shift in the difference between the Sudakov and the one-loop calculations. Also, since we always require $\sqrt{s} \gg m'$, it pushes forward the energy range where the expansion is accurate.

As a consequence of these remarks, the difference between the full one-loop MSSM effect and the Sudakov approximation is expected to be a small, slowly varying function of the energy, at least in the considered energy range. On the contrary, in the standard model, all masses are quite light compared to the typical 500–1000 GeV parton energy and we can hope to observe a better accuracy of the Sudakov expansion.

All these expectations are confirmed by actual calculations. As an illustration, we show in Fig. 5 the comparison between the full one-loop and the Sudakov calculations of the effect in the distribution $d\sigma/ds$. The left panel shows the standard model case. The right panel shows the LS2 MSSM scenario, which is the lightest considered. For purpose of comparison, we have switched off QED radiation and set $M_\gamma = M_Z$. We have computed the effects up to unrealistic values (2 TeV) of the energy, just to emphasize the convergence at high energy. The Sudakov approximation is evaluated with a common scale $\tilde{M}$ in the double and single logarithms. The best value of $\tilde{M}$ is an important issue and will be discussed below. The main features of the figure are the following.

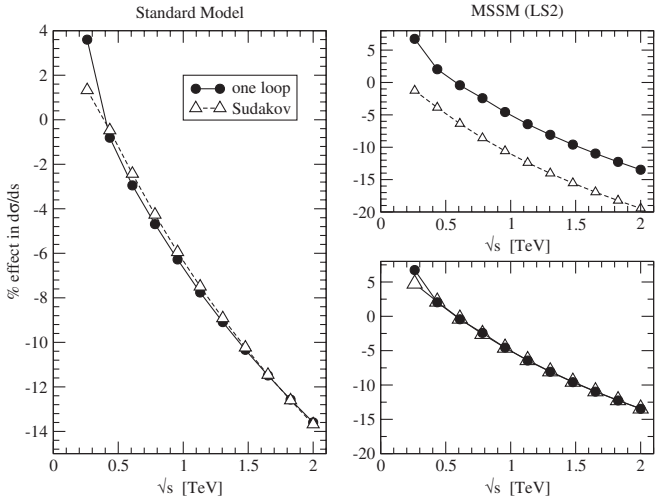

FIG. 5. Comparison between the full one-loop and Sudakov calculations of the effect in the distribution $d\sigma/ds$. The left panel shows the standard model case. The right panel shows the LS2 MSSM scenario, which is the lightest considered. In the upper figure we show the two curves, whereas in the lower panel, we have shifted the Sudakov effect by a constant $+6\%$. For purposes of comparison, we have switched off QED radiation and set $M_\gamma = M_Z$.

(a) In the standard model, we choose $\tilde{M} = M_W$. We observe a remarkable agreement. The expansion is rather accurate down to energies $\sqrt{s} \simeq 500$ GeV. The relevant scale is the electroweak breaking one $\simeq M_W$ and there are no large constant (energy independent) contributions.

(b) In the LS2-MSSM case, we adjust $\tilde{M}$ in order to have the same slope in the two curves. We have found the optimal value $\tilde{M} = 120$ GeV. With this choice, there is a large but constant shift of about $+6\%$ with respect to the Sudakov calculation as shown in the upper right panel where we show the two curves. To emphasize the energy independence of the shift, we show in the lower right panel the same one-loop curve together with a shifted version of the Sudakov one which has been moved upward by a constant $+6\%$. The agreement is again remarkable, exactly like in the standard model case.

In principle, these features could be useful if one were interested in preparing a complete NLO parametrization of the process, that includes QCD effects and decay simulation by Monte Carlo. The expected smoothness of the radiative effects beyond thresholds can be exploited to replace the full calculation by simple (model dependent) interpolating expressions. This is particularly relevant in the SM case where the Sudakov-like parametrization of the process is fixed and does not depend on any model parameter, but only on the kinematical cuts.

This remark concludes our presentation of the unpolarized effects. We move now to the discussion of the possible polarized observables of the process.

B. Polarized observables

1. Final top asymmetry: One-loop effects in A_{LR}

A special property of the tW^- production process is the fact that, in principle, the polarization of the final top quark and/or W boson can be measured. This fact, that was first considered in a previous reference [22], leads to the introduction of new observables, that we shall try to list and to discuss in what follows. The first possibility is that of measuring the final top polarization. In the process that we are considering, the final top can have in principle both helicities, as one can see from the expressions of the helicity amplitudes given in Sec. III. In correspondence to the two possible choices, we shall define two different differential cross sections, that we shall define as $d\sigma_{L,R}/ds$, that are the analogues of Eq. (47) where only the contributions from the two types of final top have been retained. Plotting these quantities at variable $\sqrt{s}$, as we did for the total unpolarized cross section, would lead to conclusions that do not much differ from those already given in the previous part of this Section: the *genuine* SUSY effect is still rather modest. Again, the overall MSSM effect is, though, not small. This could be seen in the plots of the two distributions, but from our previous discussion we believe that it might be preferable to consider, again, ratios of cross sections. With this aim, we have defined the ratio of the integrated cross sections asymmetries, i.e. the quantity

$$A_{LR}(s) = \frac{\sigma_L(s) - \sigma_R(s)}{\sigma_L(s) + \sigma_R(s)}, \quad \text{with}$$
$$\sigma_{L,R}(s) = \int_{E^2_{\text{threshold}}}^{s} \frac{d\sigma_{L,R}}{ds'} ds'. \tag{51}$$

Figures 6 and 7 show the values of A_{LR} at variable $\sqrt{s}$. One sees that, considering a realistic value e.g. $\sqrt{s} = 500$ GeV,

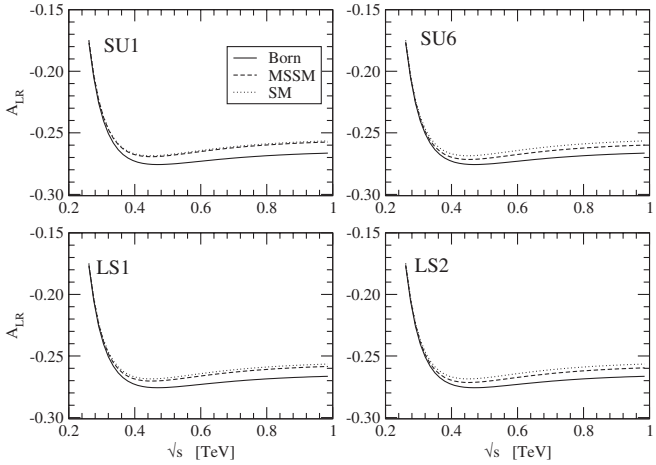

FIG. 6. Born value and MSSM/SM one-loop effect in the asymmetry A_{LR} in the four considered scenarios SU1, SU6, LS1, LS2. The cross sections entering A_{LR} are integrated from threshold up to $\sqrt{s}$.

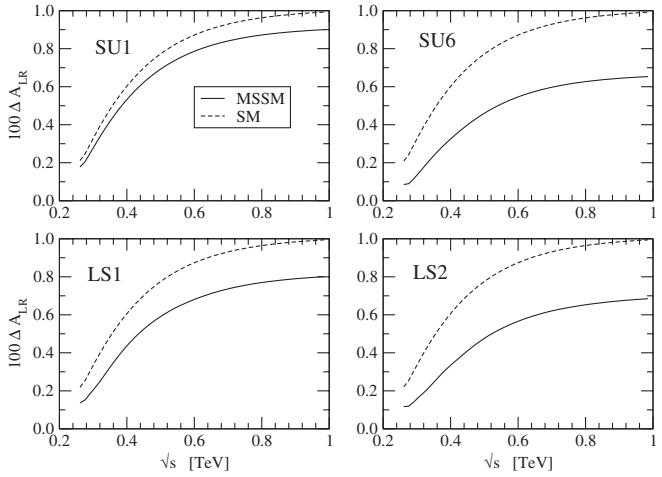

FIG. 7. Percentual MSSM and SM one-loop effect in the asymmetry A_{LR} in the four considered scenarios SU1, SU6, LS1, LS2. The cross sections entering A_{LR} are integrated from threshold up to $\sqrt{s}$.

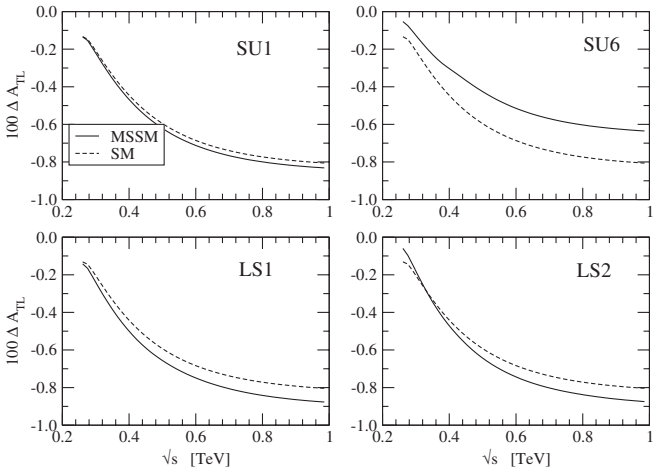

FIG. 9. Percentual MSSM and SM one-loop effect in the asymmetry A_{TL} in the four considered scenarios SU1, SU6, LS1, LS2. The cross sections entering A_{TL} are integrated from threshold up to $\sqrt{s}$.

the one-loop effect on the asymmetry reaches in all considered SUSY scenarios an absolute value of slightly less than 1%. This number should be compared to the realistic overall uncertainty. For the reasons that we have discussed previously, we expect essentially a dominance of the purely statistical experimental error, whose size will depend on the available integrated luminosity. Lacking a dedicated experimental analysis (in preparation), we can use as a guidance the preliminary quoted value (for a different single top production process, the t-channel one) of [22], that is a (mainly statistical) 4%.

2. *Final W asymmetry: One-loop effects in* A_{TL}

In the tW^- production process, the final W^- is real. Therefore one can, in principle, measure the primary W polarization. Assuming that this is the case, we have defined two quantities that are the analogues of Eq. (51) and, starting from them we have introduced the transverse-longitudinal asymmetry, defined as

$$A_{TL}(s) = \frac{\sigma_{W_T}(s) - \sigma_{W_L}(s)}{\sigma_{W_T}(s) + \sigma_{W_L}(s)}, \quad \text{with}$$
$$\sigma_{W_{T,L}}(s) = \int_{E^2_{\text{threshold}}}^{s} \frac{d\sigma_{W_{T,L}}}{ds'} ds'. \tag{52}$$

The numerical values of A_{TL} are shown in Figs. 8 and 9. In all cases the one-loop effect at the point $\sqrt{s} = 500$ GeV has an absolute value of about 0.5%. We do not have yet at disposal a suitable experimental analysis for this asymmetry, that is in fact being carried on [17].

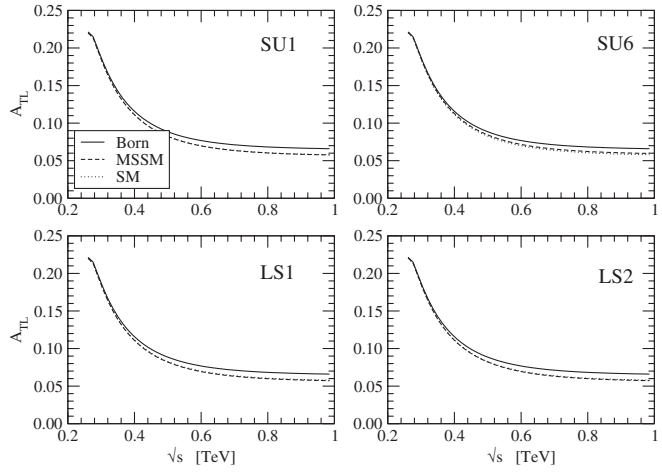

FIG. 8. Born value and MSSM/SM one-loop effect in the asymmetry A_{TL} in the four considered scenarios SU1, SU6, LS1, LS2. The cross sections entering A_{TL} are integrated from threshold up to $\sqrt{s}$.

VI. CONCLUSIONS

In this paper, we have performed the first complete electroweak one-loop analysis of the associated tW production process in the MSSM with mSUGRA mechanism of SUSY symmetry breaking. This has been done using a numerical program, MINSTREL, that satisfies the three constraints of cancellation of ultraviolet and infrared divergences and of reproduction of asymptotic Sudakov expansions. We have considered various experimental potential observables, both for unpolarized and for polarized production. We have found a relatively small genuine SUSY effect for the representative SUSY benchmark points that we have selected, and a possibly appreciable, mostly of SM origin, overall one-loop effect. We have proposed a number of new observables, in general ratios of experimentally measurable quantities, that would be essentially free of disturbing theoretical QCD and experimental systematic uncertainties. For these quantities, the predictions of the MSSM would be rather precise, making

them appear as possible precision tests of the involved genuine electroweak content of the model. The extension of our results to a different MSSM scenario or to different SUSY models would be straightforward. The still missing corresponding experimental analysis of the various proposed observables of the process is being carried on, and will appear in a more complete forthcoming paper [17].

ACKNOWLEDGMENTS

We thank C. Carloni Calame, G. Montagna, O. Nicrosini, and F. Piccinini for discussions and suggestions about the treatment of QED soft radiation and the related infrared cancellation properties.

[1] M. Beneke *et al.*, in Proceedings of the Workshop on standard model Physics (and More) at the LHC (First Plenary Meeting), Geneva, Switzerland, 2000, edited by G. Altarelli and M. L. Mangano (unpublished); CERN Report No. CERN-TH-2000-004, 2000; hep-ph/0003033.
[2] M. Beccaria, F. M. Renard, and C. Verzegnassi, Phys. Rev. D **71**, 033005 (2005).
[3] T. M. P. Tait, Phys. Rev. D **61**, 034001 (2000).
[4] A list of useful results is contained in the appendices of the paper W. Hollik and C. Schappacher, Nucl. Phys. **B545**, 98 (1999).
[5] T. Hahn, Comput. Phys. Commun. **140**, 418 (2001); T. Hahn and C. Schappacher, Comput. Phys. Commun. **143**, 54 (2002).
[6] G. 't Hooft and M. J. G. Veltman, Nucl. Phys. **B153**, 365 (1979).
[7] S. Weinberg, *The Quantum Theory of Fields*, Foundations, Vol. 1 (Cambridge University Press, Cambridge, 1995), ISBN 0521550017.
[8] M. Lemoine and M. J. G. Veltman, Nucl. Phys. **B164**, 445 (1980).
[9] M. Beccaria, C. Carloni Calame, G. Macorini, G. Montagna, O. Nicrosini, and F. Piccinini (unpublished).
[10] M. Beccaria, M. Melles, F. M. Renard, S. Trimarchi, and C. Verzegnassi, Int. J. Mod. Phys. A **18**, 5069 (2003).
[11] G. J. Gounaris and F. M. Renard, Phys. Rev. Lett. **94**, 131601 (2005).
[12] T. Hahn and M. Perez-Victoria, Comput. Phys. Commun. **118**, 153 (1999).
[13] see e.g. R. K. Ellis, W. J. Stirling, and B. R. Webber, *QCD and Colliders Physics*, edited by T. Ericson and P. V. Landshoff (Cambridge University Press, Cambridge, 1996).
[14] A. D. Martin, R. G. Roberts, W. J. Stirling, and R. S. Thorne, contribution to XI International Workshop on Deep Inelastic Scattering, St. Petersburg, 2003, hep-ph/0307262. General information and updated numerical routines for parton distribution functions can be found on the www site http://durpdg.dur.ac.uk/hepdata/.
[15] T. Sjöstrand, P. Edén, C. Friberg, L. Lönnblad, G. Miu, S. Mrenna, and E. Norrbin, Comput. Phys. Commun. **135**, 238 (2001).
[16] M. Beccaria, S. Bentvelsen, M. Cobal, F. M. Renard, and C. Verzegnassi, Phys. Rev. D **71**, 073003 (2005).
[17] M. Cobal *et al.* (unpublished).
[18] ATLAS, ATLAS Data Challenge 2 DC2 points, http://paige.home.cern.ch/paige/fullsusy/romeindex.html.
[19] A. Djouadi, J. L. Kneur, and G. Moultaka, hep-ph/0211331.
[20] J. Campbell and F. Tramontano, Nucl. Phys. **B726**, 109 (2005).
[21] E. L. Berger, T. Han, J. Jiang, and T. Plehn, Phys. Rev. D **71**, 115012 (2005).
[22] B. Gonzalez Pineiro, D. O'Neil, R. Brock, and M. Lefebvre, CERN Report No. ATL-PHYS-2000-017, 2000.